TED-AJ03-582

NUMERICAL AND EXPERIMENTAL STUDY ON TURBULENT THERMAL MIXING IN A T-JUNCTION FLOW

NAOYA FUKUSHIMA[1], KOJI FUKAGATA[1,2], NOBUHIDE KASAGI[1]
[1]Dept. of Mech. Eng., The University of Tokyo, 7-3-1 Hongo, Bunkyo-ku, Tokyo 113-8656, Japan
[2]Inst. for Energy Utilization, AIST, 1-2 Namiki, Tsukuba-shi, Ibaraki 305-8564, Japan
E-mail: fukusima@thtlab.t.u-tokyo.ac.jp, fukagata@thtlab.t.u-tokyo.ac.jp, kasagi@thtlab.t.u-tokyo.ac.jp

HIRONORI NOGUCHI[3], KOICHI TANIMOTO[3]
[3]Mitsubishi Heavy Industries, LTD., 2-1-1 Shinhama, Arai-cho, Takasago, Hyogo 676-8686, Japan
E-mail: hironori_noguchi@n.trdc.mhi.co.jp, kouichi_tanimoto@n.trdc.mhi.co.jp

Keywords: Turbulent Mixing, T-junction, Numerical Simulation, Experiment

ABSTRACT

Thermal fatigue of the structure around a T-junction is a technically important issue for the safety of nuclear power plants. The cause for this is related to mixing of hot and cold fluids, though detailed mechanisms and effects of various parameters on those are still unclear. In the present study, direct numerical simulation (DNS) and experiments of flow in two square ducts connected via a T-junction, as shown in Fig. A1, are carried out. The Reynolds number of the main stream based on the bulk mean inlet velocity and the hydraulic diameter is about 4485. The hydraulic diameter of the branch duct is a half of that of the main duct. The velocity ratio of the branch jet to the main stream, V_r, is 2. Due to computational cost, a lower Prandtl number (Pr=0.71) is used in DNS as compared to those in experiments (Pr=2.6~8.8). Five different Richardson numbers (Ri=g$\alpha\Delta T\delta/U_{bl}^2$=0, ±0.93, ±9.3; +: stable, -: unstable) are examined to investigate effects of buoyancy on the turbulent velocity and temperature fields, especially on temperature fluctuations on the walls. Three types of grid systems are used to investigate dependency on the mesh size and the domain size. Nine corresponding cases of experiments are carried out in order to obtain verification data for DNS. Laser Doppler Velocimeter (LDV) and thermocouples are used to measure velocity and temperature, respectively.

Mean and RMS velocities in the main-flow and vertical directions and temperature from the simulation with the fine grid system agree quantitatively well with the experiments in the neutral case. Flow visualization reveals that the skewed temperature fluctuations on the duct walls are caused by various kinds of large-scale coherent structures near the T-junction, such as a groove on the branch jet, upper and lower kidney vortices, separation in the branch duct and roll-ups shed from the leading and trailing edges of the duct.

The buoyancy dramatically alters the mean velocity and temperature distribution in the strongly stable/unstable case (Ri=±9.3), whilst its effects are localized at Ri=±0.93. As shown in Fig. A2, the magnitude of temperature fluctuations downstream on the bottom wall is the largest in the case without buoyancy. The reason is found to be as follows. In the stable cases, relatively small penetration rates of the branch jet to the bottom wall lead to stratification. In the unstable cases, the condition changes into a stable state near the bottom wall once the cold fluid from the branch jet goes under the hot main stream. Those stabilizing mechanisms are missing in the neutral case.

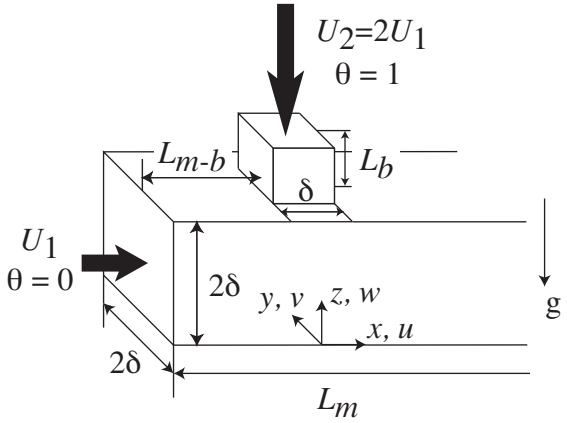

Fig. A1 Flow geometry and coordinate system

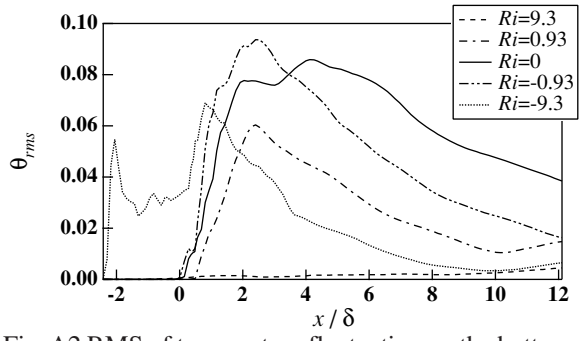

Fig. A2 RMS of temperature fluctuation on the bottom wall (y/δ=1.0)

Copyright © 2003 JSME

NOMENCLATURE

c_p specific heat at constant pressure
g gravitational acceleration
Pr Prandtl number
Re Reynolds number
Ri Richardson number
T temperature
t time
u, v, w velocity components (see, Fig. A1)
u_τ friction velocity
V_r inlet velocity ratio, U_2/U_1
x, y, z Cartesian coordinates (see, Fig. A1)

Greek Symbols
α coefficient of volumetric expansion
δ hydraulic diameter of branch duct
κ thermal diffusivity
μ dynamic viscosity
ν kinematic viscosity
ρ density
θ dimensionless temperature

Subscripts
b bulk
1 value of main duct or stream
2 value of branch duct or jet

INTRODUCTION

Clarification of criteria for the occurrence of high-cycle thermal fatigue around a T-junction part in the piping system is one of the important technical issues for the safety of nuclear power plants. This high-cycle fatigue is caused by flow-originated large-scale temperature fluctuations on the wall. Therefore, understanding of the generation mechanism of temperature fluctuations in the fluid is of the greatest importance.

For this problem, several experimental studies are conducted. In Japan, a utility-vendor joint research project on thermal striping in mixing tees with hot and cold water has been conducted [1]. Based on the results obtained there, design guidelines for piping of LWR (Light Water Reactor) plant will be discussed and drawn up by a working group in the Japan Society of Mechanical Engineers.

Despite the maturity of the numerical simulation technique and the explosive development of computers, only a few attempts have been made to clarify such mechanisms by means of numerical simulation. Sierra-Espinosa *et al*. [2] performed simulation of T-junction water flow by using turbulence models. They examined different turbulence models such as k-ε, RSM and RNG models. The computational predictions with any turbulence models examined, however, showed significant discrepancy with experimental measurement. This suggests that, at the present stage, one should employ direct numerical simulation (DNS), or possibly large eddy simulation (LES), for the prediction of this type of complex flow. Although pseudo-DNS and LES of the turbulent T-junction flow is reported by Simoneau *et al*. [3] for a sodium flow related to fast reactors, it is difficult to judge whether the obtained results are reliable since the numerical errors in the CFD package used cannot be evaluated.

Therefore, in the present study, DNS of T-junctioned square duct flow is performed on a solid base. The DNS code used here has been validated for a straight square duct flow [4]. We also conduct experiments in order to validate the computational result. Those numerical and experimental data are used to investigate the mechanism of the occurrence of the large-scale temperature fluctuations. Our final goal is to clarify the important mechanisms and to propose safety criteria as mentioned above. Here we mainly focus on the fundamental vortex dynamics around the T-junction and influence of buoyancy on the flow pattern.

EXPERIMENTAL SETUP

In order to obtain verification data for DNS, experiments of thermal striping in the mixing zone with square ducts are carried out. The velocity and the temperature are, respectively, measured by Laser Doppler Velocimetry (LDV) and thermocouples.

The main duct is arranged in the horizontal direction and the branch duct is attached upright, as shown in Fig. 1. Both the main duct and the branch duct have square cross-sections with sides of 100mm and 50mm, respectively. These ducts are made of acrylic resin suitable for visualiza-

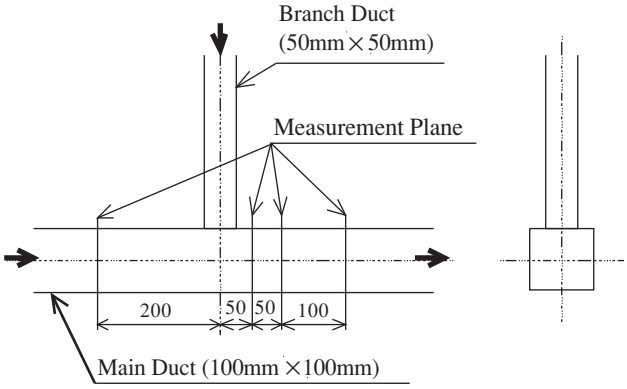

Fig. 1 Test section

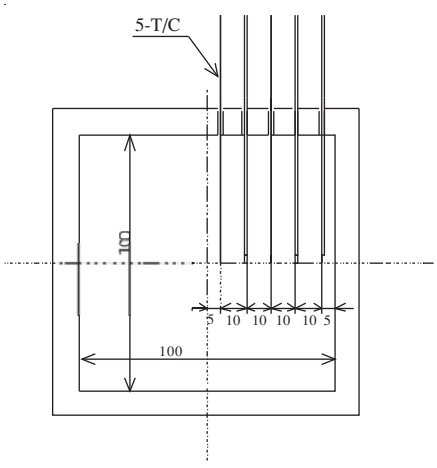

Fig. 2 Thermocouples tree

Copyright © 2003 JSME

Table 1 Test matrix for temperature measurement

	Main duct				Branch duct					
	U_1 (m/s)	T_1 (° C)	Re	Pr	U_2 (m/s)	T_2 (° C)	Re	Pr	ΔT (° C)	Ri
Case 1	0.02	70.32	4840	2.6	0.04	27.42	2370	5.8	-42.9	-11.0
Case 2	0.02	28.55	2400	5.7	0.04	69.44	4840	2.6	40.89	10.5
Case 3	0.02	34.59	2740	5.0	0.04	26.43	2290	6.0	-8.16	-2.10
Case 4	0.02	28.53	2400	5.7	0.04	35.82	2740	5.0	7.29	1.88
Case 5	0.15	70.48	36300	2.6	0.3	23.78	16300	6.3	-46.7	-0.214
Case 6	0.15	23.83	16300	6.3	0.3	70.21	36300	2.6	46.38	0.212

Table 2 Test matrix for velocity measurement

	Main duct				Branch duct					
	U_1 (m/s)	T_1 (° C)	Re	Pr	U_2 (m/s)	T_2 (° C)	Re	Pr	ΔT (° C)	Ri
Case 1´	0.02	20	2000	6.9	0.04	20	2000	6.9	0	0
Case 3´	0.02	19	2000	6.9	0.04	11.5	1540	8.7	-7.5	-1.93
Case 5´	0.1	16.89	8790	7.5	0.2	11	7500	8.8	-9	-0.093

tion. Flow straighteners are installed at 20 hydraulic diameters upstream of each side from the mixing point. The experiments are conducted under atmospheric pressure. Hot and cold water are supplied to the main and branch ducts.

The velocities in the streamwise and vertical directions are measured by LDV in measurement planes. Five thermocouples are installed like trees as shown in Fig. 2 and are traversed in the vertical direction from the bottom to the top. These thermocouple trees are located at x=-200mm, 50mm, 100mm and 200mm. C-A thermocouples have a 0.5mm sheath diameter and are the non-ground connection type.

The test matrices for the temperature and velocity measurement are shown in Tables 1 and 2, respectively. The velocity ratio, V_r, is 2.0 and the inlet temperature difference is varied from 0 to 47 °C. In Cases 5, 6 and 5', the magnitude of both inlet velocities is respectively 7.5, 7.5 and 5 times as high as other cases in order to reduce the effect of buoyancy. These are compared with the neutral case in the numerical simulation. In the velocity measurement by LDV, the temperature difference is reduced to avoid the refractive index difference of the hot and cold water. The temperature is sampled at 50Hz with a sampling period of 12 minutes while. The velocities are measured for 10 minutes at 50Hz sampling rate.

Both the Reynolds numbers and the Prandtl numbers vary with the temperature mainly because the dynamic viscosity of water is highly dependent on the temperature. It should be noted that the Reynolds numbers in Cases 1' and 3' are very low and the flows are in the transition range.

NUMERICAL PROCEDURE

In the present study, the flow is assumed to be incompressible. The buoyancy force due to the temperature difference is incorporated by adding a body force term to the Navier-Stokes equation based on the Boussinesq approximation. Since reasonably fine computational mesh is used as described below, no turbulence model is used. The dynamic viscosity, μ, the specific heat at constant pressure, c_p, and the thermal diffusivity, κ, are set constant in the simulation, while in reality they, particularly μ, are temperature-dependent quantities, as described in the previous section.

The DNS code used in the present study is based on that used for a turbulent straight square duct flow [4]. Basically, the spatial discretization is done by the second-order accurate finite difference method. As an exception, the TVD scheme is adopted for the advection term in the temperature equation in order to avoid numerical instability due to possible overshoot/undershoot. The time integration is done by the third-order accurate low storage Runge-Kutta/Crank-Nicolson (RK3/CN) scheme similar to that used by Rai & Moin [5].

The flow geometry and the coordinate system used are shown in Fig. A1. The computational domain is $L_m \times 2\delta \times 2\delta$ in the directions of main flow (x), width (y) and height (z) for the main duct, and $\delta \times \delta \times L_b$ for the branch duct. The branch duct is connected to the main duct via a T-junction L_{m-b} downstream of the main inlet. The origin of the coordinate system is located at the bottom corner of the main duct in the center plane of the branch duct. Three types of the computational domain and number of grids are given in Table 3. Cases CS and CL have coarse grid systems. The difference is the upstream length of the main and branch ducts. In Case F, a fine grid system is used.

The time-dependent inlet velocity fields are given by DNS of fully developed turbulent flows in periodic square ducts run simultaneously. The velocity ratio, U_2 / U_1, is 2. The bulk Reynolds number, $\mathrm{Re_b} = U_1(2\delta)/\nu = U_2\delta/\nu$, is 4485 at both inlets. This Reynolds number differs from those in the experiments due to the constant dynamic viscosity assumed in the simulation. The dimensionless temperature, $\theta = (T - T_1)/\Delta T$, where $\Delta T = T_2 - T_1$, is zero at the

Copyright © 2003 JSME

Table 3 Basic computational conditions

	Main duct		Branch duct		
	Domain	Numbers of Grid	Domain	Numbers of Grid	$L_{m\text{-}b}$
Case CS	$14.6\delta \times 2\delta \times 2\delta$	$128 \times 69 \times 65$	$\delta \times \delta \times 0.92\delta$	$15 \times 15 \times 16$	1.97δ
Case CL	$30.3\delta \times 2\delta \times 2\delta$	$256 \times 69 \times 65$	$\delta \times \delta \times 8.8\delta$	$15 \times 15 \times 144$	17.67δ
Case F	$14.2\delta \times 2\delta \times 2\delta$	$224 \times 145 \times 65$	$\delta \times \delta \times 2.1\delta$	$65 \times 65 \times 48$	3.0δ

main inlet and unity at the branch inlet. At the outlet, the convective outlet condition similar to that used by Le & Moin [6] is applied. Due to computational cost, a Prandtl number of Pr=0.71 is used in the simulation, which is lower than those in the experiments (Pr=2.6~8.8) shown in Tables 1 and 2. At the walls, no-slip and adiabatic conditions are imposed as velocity and temperature boundary conditions.

In the present study the Richardson number is defined as

$$Ri = \frac{g\alpha\Delta T\delta}{U_1^2} \tag{4}$$

and the effects of buoyancy are studied for five cases, i.e., Ri=0, ±0.93, ±9.3 only in Case CS. The neutral condition corresponds to Cases 5 and 6 in Table 1 and Cases 1' and 5' in Table 2. The other conditions correspond to Cases 1 - 4 in Table 1, respectively. The absolute values of the Richardson numbers in Cases 3, 4 and 3' (in the experiments) are nearly twice as large as those in the corresponding simulation. The reason is the failure to keep to the originally intended small inlet temperature of 4 °C. Note that positive values of the Richardson numbers correspond to cases where the temperature at the branch inlet is higher than that of the main inlet, such as Case 2 in Table 1. Hereafter we call these cases as stable cases. On the other hand, cases with negative values of the Richardson numbers, such as Case 1, are referred to as unstable cases.

RESULT AND DISCUSSIONS

Comparison between experiment and simulation

Several mean flow and thermal properties obtained from the simulation and the measurement are compared in this section. On account of limited space, only the case of $Ri \approx 0$, where velocity and temperature properties are measured both in the simulation and the experiments, is shown here.

First, comparisons between the fine grid simulation and the experiments are presented. The mean and root-mean-square (RMS) velocities in the main-flow and vertical directions, and temperature at three different downstream locations are shown in Figs. 3 (a), (b) and (c), respectively, as functions of the height, z. These values are sampled at y/δ=0.7.

In the previous study, Kelso *et al*. [7] pointed out drastic changes in vortex structures from a laminar flow to turbulence in their experimental study of a round jet in a crossflow on a boundary layer. Takahashi *et al*. [8] showed only a slight dependence of thermal mixing characteristics around T-junction on their Reynolds numbers as far as the flow is turbulent. Therefore we carried out two experiments in almost a laminar flow (Case 1') and in turbulence (Case 5'). As shown in Figs. 3 (a) and (b), all the mean and RMS velocities in Case F agree with those in Case 5' fairly well both qualitatively and quantitatively everywhere in spite of the difference in the Reynolds numbers. On the other hand, the mean and RMS velocity profiles in Case 1' largely deviate from those in Case 5' and Case F. Similar tendencies to the previous studies are observed.

Distribution of the mean and RMS temperature in the simulation and in two experiments at the higher Reynolds numbers, with the slight difference in the Richardson numbers, is shown in Fig. 3 (c). They are in both qualitative and quantitative agreement only right downstream of the branch exit (x/δ=1). The effects of buoyancy in two experiments are obvious only farthest downstream (x/δ=4) among the measurement points. Therefore, the deviations of the mean and RMS temperature at x/δ=2 between two experiments and the simulation are attributed to the difference in the Prandtl numbers. At higher Prandtl numbers, a thinner mixing layer of temperature causes larger temperature fluctuations.

Dependency on mesh size and length from the inlets is shown in Fig. 4. The vertical mean velocity and the RMS temperature at y/δ=0.5 are plotted as samples because they are more dependent on the computational conditions than other variables. The simulation with the coarse grid systems (Cases CS and CL) has only qualitative agreement with the experiments and underestimates both values. The coarse grid systems are enough only to carry out qualitative investigations. Improvement is achieved in Case F. On the other hand, there is no improvement in Case CL. It is already pointed out by Andreopoulos [9] that there is an influence of a crossflow over a boundary layer on a jet still in a pipe, which corresponds to the branch duct in the present study, and that a separation region is formed in the leading edge of the pipe, especially at low velocity ratios. The jet trajectory would be strongly affected by the separation region. Therefore the mesh size must be fine enough to capture the separation region [10]. However, the ones in Cases CS and CL are not adequately fine.

Effects of buoyancy on the flow structure

In this subsection, dependence of flow patterns on the Richardson numbers and mechanisms of formation of the temperature fluctuations are qualitatively discussed. The data used in this section are obtained from the numerical simulation of Case CS. It should be kept in mind that the velocities and temperature obtained in Case CS agree with those in the experiments only qualitatively and that the lower

Copyright © 2003 JSME

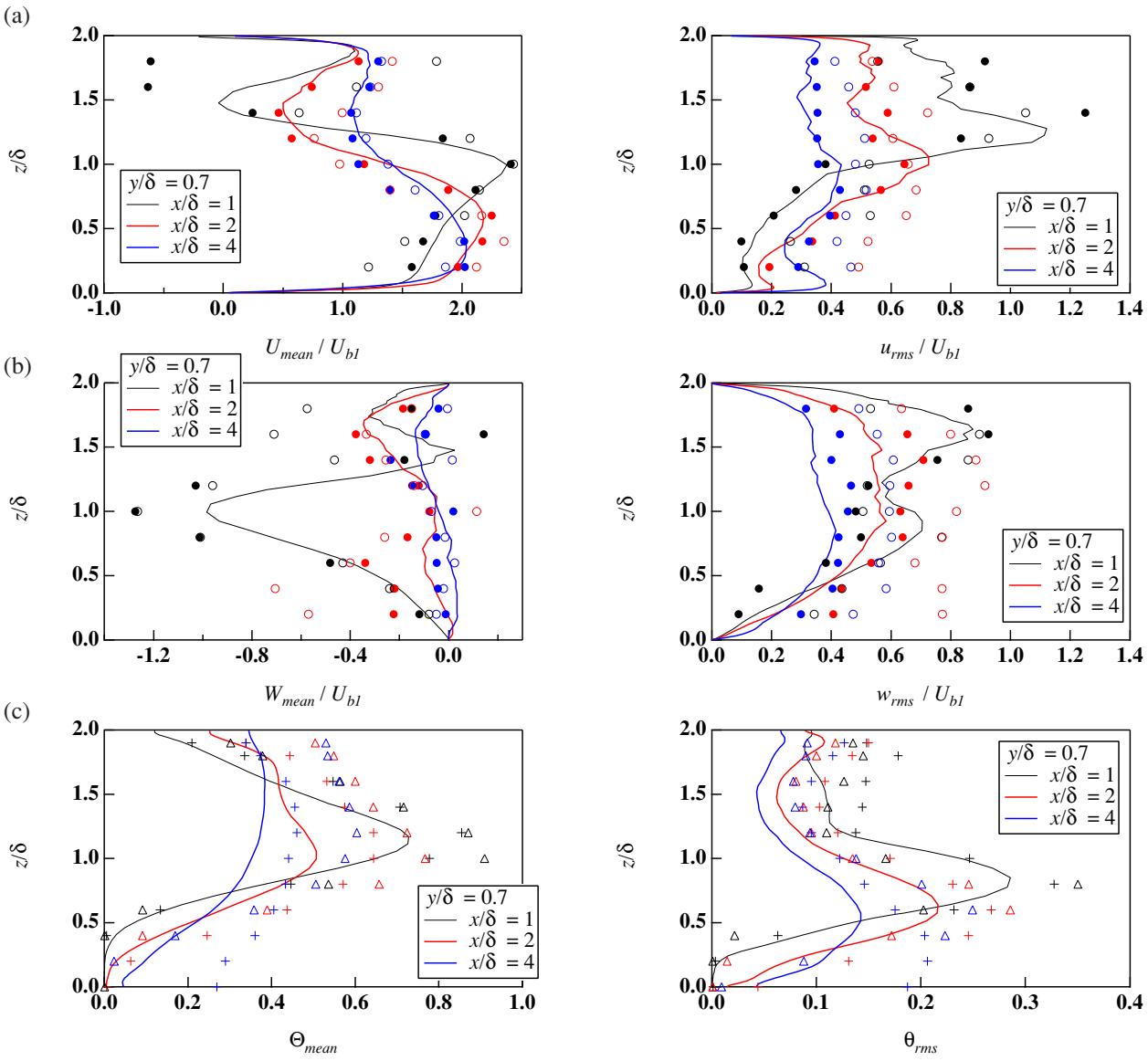

Fig. 3 Comparison between numerical data obtained with a fine grid system (solid lines) and experimental data (symbols) at y/δ=0.7 in the case of Ri≈0: (a) velocity in the direction of main flow; (b) vertical velocity; (c) temperature. ○: Case 1', ●: Case 5', +: Case 5, △: Case6. Left: mean value and right: RMS.

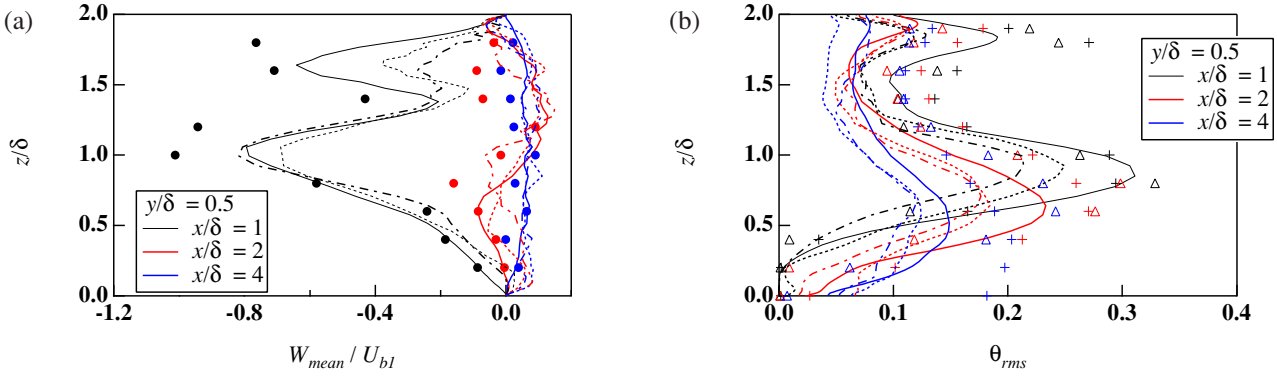

Fig. 4 Comparison between numerical data (lines) and experimental data (symbols) at y/δ=0.5 in the case of Ri≈0: (a) mean vertical velocity; (b) RMS of temperature. ——: Case F, - - - : Case CS, — - —: Case CL. ●: Case 5', +: Case 5, △: Case6.

Copyright © 2003 JSME

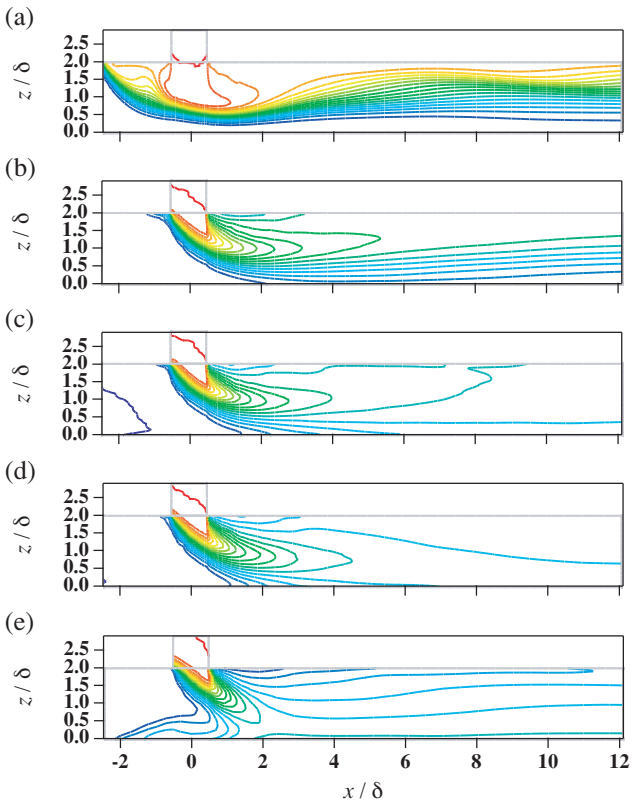

Fig. 5 Contours of mean temperature in the center plane (y/δ=1.0). The increment is 0.05. (a) Ri=9.3; (b) Ri=0.93; (c) Ri=0; (d) Ri=-0.93; (e) Ri=-9.3.

Prandtl number in the simulation underestimates the effects of stratification. This underestimation is caused by smaller buoyancy force resulting from more rapid diffusion and from a thicker mixing layer of temperature. Similar phenomena are observed in stably-stratified mixing layers [11].

Figure 5 shows the contours of the mean temperature in the center plane for different Richardson numbers. In the strongly stable case (i.e., Ri=9.3), the hot branch jet cannot penetrate the cold main flow. The branch jet is pushed aside around the T-junction part and the temperature is stably stratified in the downstream region. In the neutral case (Ri=0), the mean temperature is homogeneous downstream. This indicates that active mixing of main and branch flows occurs around the T-junction part. An interesting behavior is observed in the strongly unstable case (Ri=-9.3). Although the temperature contour around the T-junction part is similar to that in the neutral case, a stable stratification is observed downstream. This can be explained by that the cold branch jet immediately penetrates through the hot main flow to result in a situation similar to the stable case. In the weakly stable/unstable cases, the behavior is similar to that of the neutral case.

From the observation above, one can expect that the temperature fluctuations are larger when the absolute Richardson number is smaller. The root-mean-square (RMS) values of the temperature fluctuations on the bottom wall for different values of Ri are shown in Fig. 6 (a).

It is reconfirmed that the temperature fluctuations for smaller Ri are larger in the downstream region. In the strongly stable case, there is almost no fluctuation. In the strongly unstable case, the fluctuations are large around the junction part due to the inherent unstableness. In the downstream region, however, the fluctuations become smaller than those in the neutral and the weakly stable/unstable cases, which is consistent with the explanation above.

On the other hand, except for the strongly stable case, the RMS temperature fluctuations at z/δ=1.75 on the side wall (Fig. 6 (b)), where θ_{rms} has a maximum value in the neutral case of Case CS, is hardly affected by the buoyancy. Thus, the mechanisms of producing temperature fluc-

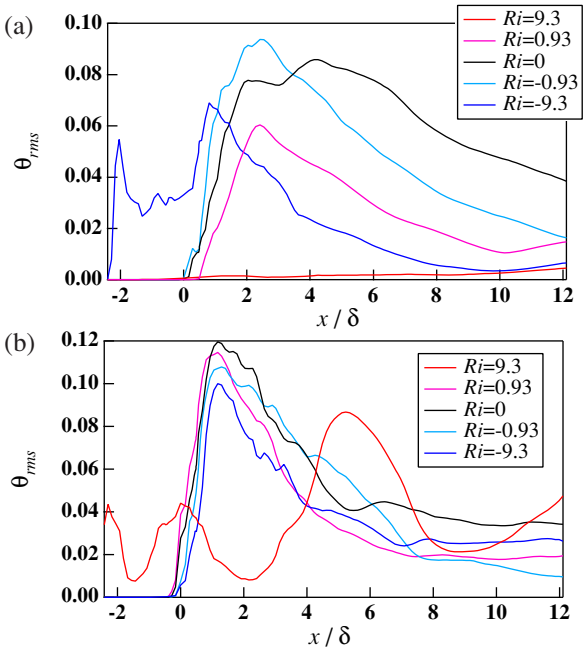

Fig. 6 RMS of temperature: (a) on the bottom wall (y/δ=1.0); (b) on the side wall (z/δ=1.75).

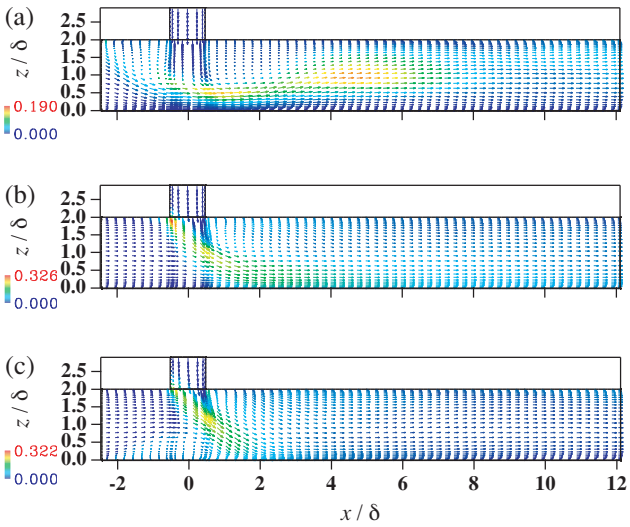

Fig. 7 RMS of temperature (color) together with mean velocity vectors in the center plane (y/δ=1.0): (a) Ri=9.3; (b) Ri=0; (c) Ri=-9.3.

Copyright © 2003 JSME

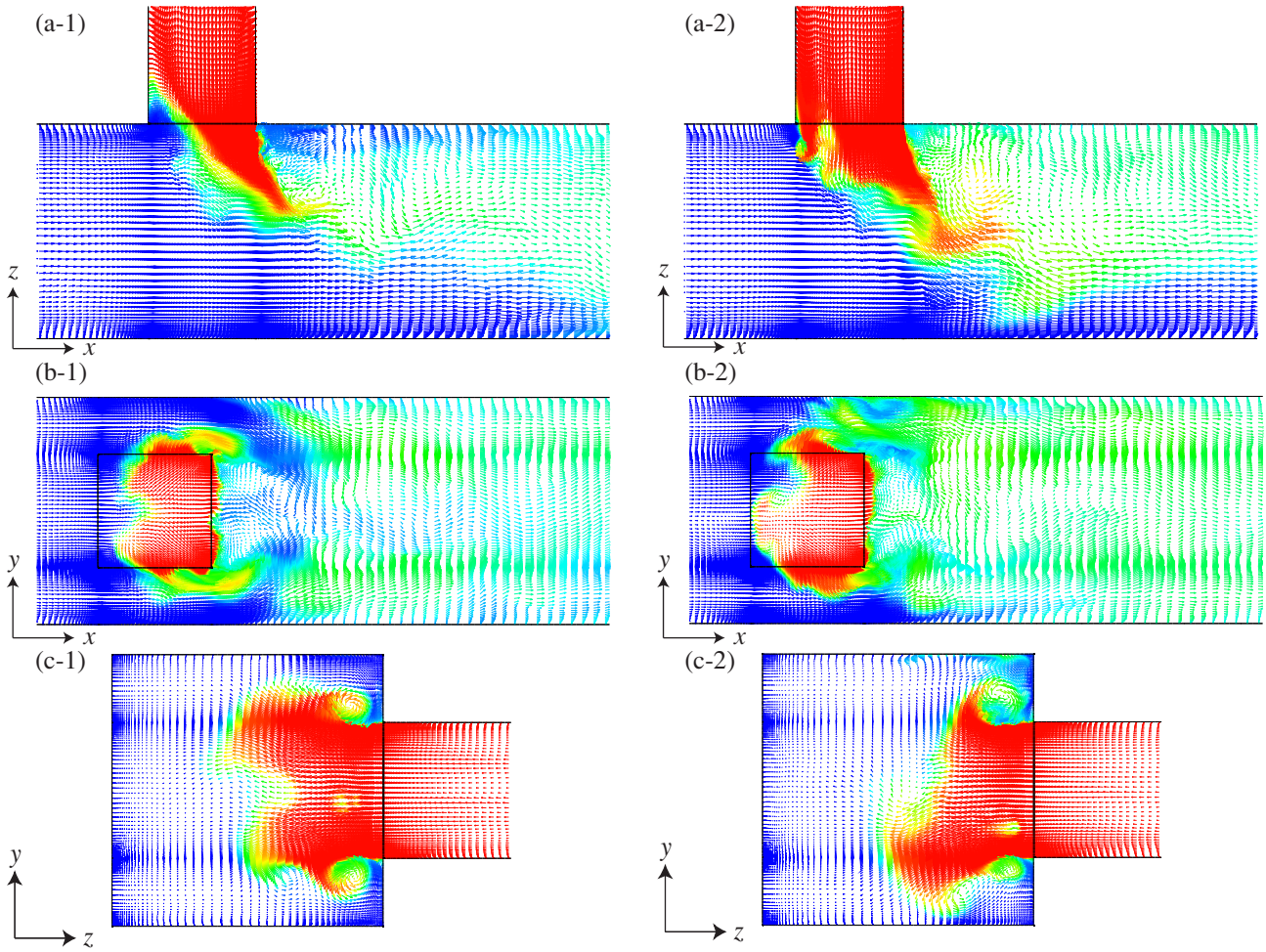

Fig. 8 Instantaneous velocity vectors and temperature fields in the neutral case. Color: from red ($\theta = 1$) to blue ($\theta = 0$). (a) x - z cross section at y/δ=1.0; (b) x - y cross section at z/δ=1.8; (c) y - z cross section at the trailing edge (x/δ=0.5). Left: t=16.1 and Right: t=19.0.

tuations would be independent of *Ri*.

The RMS temperature and mean velocity vectors in the center plane are depicted in Fig. 7. Note that the maximum RMS temperature in the strongly stable case is smaller than that in the neutral and strongly unstable cases. In all three cases, large temperature fluctuations are found near the mixing layers between the main stream and the branch jet. In the strongly stable case, the branch jet is affected only a little by the main stream and goes downward straightly. The shape of the mixing layer is comparably flat and the RMS temperature is independent of y-direction. In the neutral case, very large fluctuations can be observed near the leading edge of the junction part in addition to the bottom wall. In the strongly unstable case, the distribution of the thermal fluctuations resembles that in the neutral case. The branch jet, however, reverses upstream after it collides with the bottom wall. This explains the spreading of mean temperature near the bottom wall as observed in Fig. 5 (e).

Thermal flow dynamics

The cause of such large fluctuations in the neutral case is investigated by examining the instantaneous distribution of velocity vectors and temperature as shown in Fig. 8. This distribution is obtained from the simulation of Case F. Two instantaneous fields, i.e., at t=16.1 when the temperature at x/δ=2.0 on the bottom wall (y/δ=1.0, z/δ=0.0) is decreasing slowly after a sudden increase and t=19.0 when it is going to increase (see also Fig. 9 (c)) are shown.

In Fig. 8 (a-1), the jet that resides inside the branch duct is strongly bent by the main flow, while the main flow creeps [9] in the branch duct around the leading edge. The mixing layer between the jet and the crossflow is formed at a higher position. The main flow prevents the jet from reaching the bottom wall. Near the leading edge of the branch duct, the shear layer is relatively calm and less roll-ups are discharged, whereas vortex loops are released from the trailing edge. These phenomena are similar to the single-side vortex loops observed in the experiments of a jet in a boundary layer crossflow at low velocity ratio, typically less than one [12]. The T-junction is a confined system. The peripheral walls of the main duct prevent the crossflow from spreading as wide as a crossflow on a boundary layer. This causes the effective velocity ratio to drop. Moreover, the crossflow makes a groove from the leading to the trailing edge of the branch jet near the symmetrical plane as shown in Figs. 8 (b-1) and (c-1), which gives rise to a locally low effective

Copyright © 2003 JSME

velocity ratio. Our interpretation is that the reduced effective velocity ratio is the cause for the similarity to a jet in a crossflow at a low velocity ratio. On the other hand, the fluid flows faster in the regions aside of the groove because of the incompressibility. As a result, the effective velocity ratio increases there.

Similar states arise at t=19.0 in Figs. 8 (a-2), (b-2) and (c-2), although the groove on the branch jet moves from the middle to the left (y/δ>1.0). In the center plane, the jet is less affected by the main flow than at t=16.1 and is rushing down to the bottom wall. Such temporal variation of the position where the branch jet reaches the bottom wall causes the temperature fluctuations on the bottom wall. The separation at the leading edge in the branch duct is pushed away and the vortex loops are released. This corresponds to the previous observation that oscillations of a separation region at an upstream lip of a pipe are synchronized with roll-ups of a jet shear layer [7]. On the other hand, the roll-ups continue to be shed from the trailing edge. However, no vortex ring is formed, as pointed out in large-eddy simulation [13] and experiments [12]. Steady separation with small oscillations is found just upstream of the jet in Figs. 8 (a-1) and (a-2). It cannot grow up to a horseshoe vortex, which is observed in the experiments of a jet in a crossflow on a boundary layer (e. g., [14], [15]), because of the geometrical constraints imposed by the side walls of the main ducts. Another difference is that the steady separation in the T-junction contains only one primary vortex, whereas the one in the jet in the boundary layer crossflow contains two vortices [14].

In the cross-stream sections, almost steady lower kidney vortices are observed near the trailing edge of the branch duct (Fig. 8 (c)). In the case of a jet in a cross flow on a boundary layer, the cross flow suppresses upward and lateral spread of the jet and forces the vortices to roll up [16]. In the present case of the T-junction, kidney vortices also appear although the lateral spreading is prevented by the side walls. The fluctuating projection of the branch jet often gives rise to unsteady upper kidney and anti-kidney vortices at both sides of the projection in Fig. 8 (c-2). These vortices contribute to heat transfer parallel and normal to directions of the eruption of the branch jet. These double-decked structures are similar to those observed in experiments of a jet in a crossflow on a boundary layer by Haven *et al*. [16]. Directions of rotation of these upper-deck vortices depend on the geometry of exits of jets. For low-aspect-ratio exits, upper kidney vortices rotate with the same directions as the lower pair, while for high-aspect-ratio exits, upper anti-kidney vortices appear with the opposite directions. In the present simulation around T-junction, the upper kidney vortices predominate over the upper anti-kidney vortices, which agrees with their observations, although additional upper anti-kidney vortices can also appear at the same time. The time variation of these upper and lower vortices contributes to the temperature fluctuations on the side and top walls.

In the x-y planes (Fig. 8 (b)), vortices are observed immediately downstream of the junction part. These vortices make low and high temperature streaks meander along with the vibration of the branch jet.

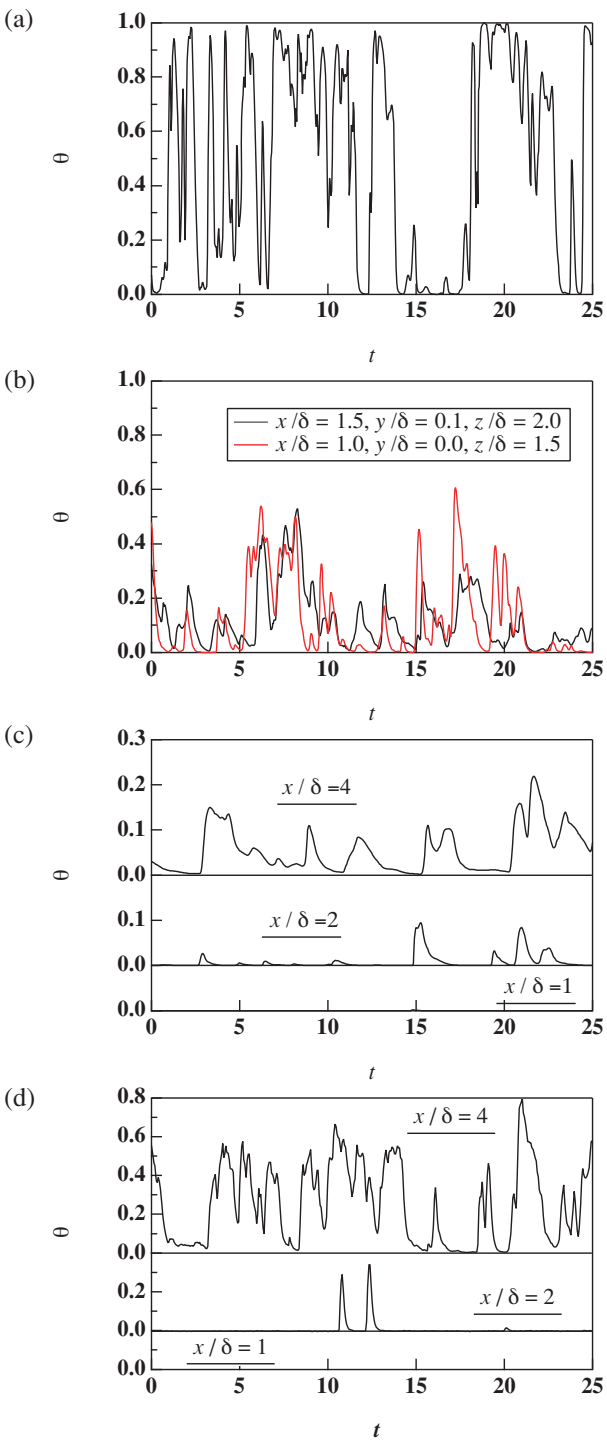

Fig. 9 Instantaneous signals of temperature at Ri≈0: (a) at the maximum RMS temperature position in the T-junction (x/δ=-0.4, y/δ=0.9, z/δ=1.9); (b) at the maximum RMS temperature positions on the top and side walls; (c) on the bottom wall (y/δ=1.0, z/δ=0.0) in the numerical simulation; (d) on the bottom wall (y/δ=0.9, z/δ=0.0) in the experiment (Case 5).

As visualized above, the temperature fluctuations on the

Copyright © 2003 JSME

duct walls are brought about by the oscillations of the groove on the branch jet in time and space, especially in y-direction, which are made by interaction between the jet and the crossflow, and by the various resultant large-scale coherent structures and their interactions.

In Fig. 9, instantaneous signals of temperature at several points in the neutral case in the simulation (Case F) and in the experiment (Case 5) are plotted against time scaled by U_1 and δ. Note that the Reynolds number in Case 5 is higher than that in the simulation to reduce the effects of buoyancy, as mentioned in the previous section, and that the signals are measured in each time period at each height in the experiment, whereas all the signals are sampled in the same time span in the simulation.

As shown in Fig. 9 (a), large temperature oscillations are found near the leading edge of the branch duct (x/δ=-0.4, y/δ=0.9, z/δ=1.9) where the RMS temperature has the maximum value in the present simulation. The peak-to-peak amplitude of the temperature reaches almost 1.

Figure 9 (b) shows instantaneous signals of temperature at the maximum RMS temperature positions on the side and top walls in the simulation, respectively. Highly similar sequences of these two signals indicate that the mechanisms of producing the thermal fluctuations at the maximum RMS temperature positions on the side and top walls are almost the same. As mentioned above, the fluctuating kidney vortices would give rise to the temperature fluctuations on these walls.

Finally, instantaneous signals of temperature on the bottom wall at three points in the main-flow direction are presented in Fig. 9 (c) (simulation) and in Fig. 9 (d) (experiment), respectively. At x/δ=1.0, both the temperature fluctuations are almost zero, which indicates that the branch jet cannot approach directly below the trailing edge of the branch jet. At x/δ=2.0, sudden increments of the temperature are observed, which suggests the existence of highly intermittent rushes of the branch jet to the bottom wall. In both the experiment and the simulation, the attachment positions of the branch jet on the bottom wall are located at between x/δ=1.0 and 2.0. The peak-to-peak amplitude reaches about 0.1 in the simulation and about 0.3 in the experiment, both of which are six times higher than the RMS temperature. Note that the RMS temperature in Fig. 6 is obtained in simulation with the coarse grid system, which is different from the present case. The peak-to-peak amplitude in the experiment is three times as high as that in the simulation due possibly to both the higher Prandtl number and the non-zero Richardson number. While the temperature is convected downstream, the mean value rises and the shape gradually becomes obscure by thermal diffusion.

Spectral analysis

In Fig. 10, one-sided power spectra of the temperature are plotted against frequency scaled by U_1 and δ. Power spectra are calculated from the data series divided in five in the simulation (Case F) and in eight in the experiment (Case 5) and are averaged. Frequency ranges from 0.004 to 8.3

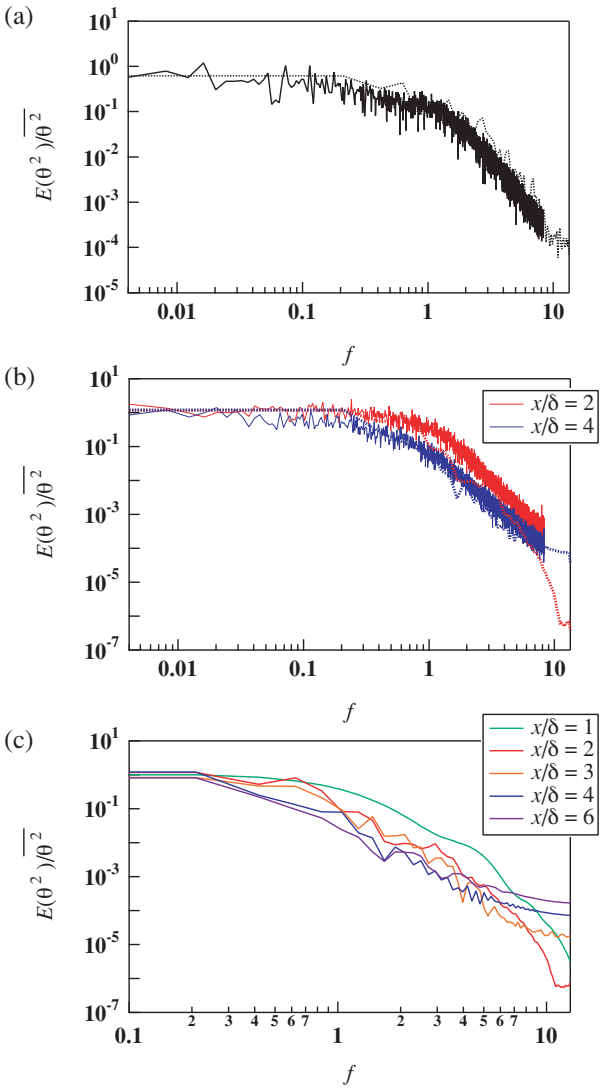

Fig. 10 One-sided power spectra of temperature at $Ri\approx0$: (a)* at the maximum RMS temperature position (x/δ=1.0, y/δ=0.9, z/δ=0.8) among measurement points; (b)* on the bottom wall for both experiment (y/δ=0.9, z/δ=0.0) and simulation (y/δ=1.0, z/δ=0.0); (c) on the bottom wall (y/δ=1.0, z/δ=0.0) for numerical simulation. *; Solid lines: experiment and Dotted lines: simulation.

in the experiment and from 0.2 to 13.4 in the simulation. In order to compensate the difference of the temperature power at each position, a one-side power spectrum is normalized by local $\overline{\theta^2}$.

The spectrum at the maximum RMS temperature position (x/δ=1.0, y/δ=0.7, z/δ=0.8), where the mixing layer is formed, is shown in Fig. 10 (a). The result in the simulation is also included in Fig. 10 (a). These data are in quantitative agreement. The spectra on the bottom wall in the simulation and the experiment are compared at x/δ=2.0 and 4.0 in Fig. 10 (b). The spectra coincide at x/δ=4.0, while the spectrum in the simulation decreases more sharply in the high frequency range than that in the experiment at x/δ=2.0. A series of spectra in x-direction on the bottom wall,

Copyright © 2003 JSME

which is obtained from the simulation, is shown in Fig. 10 (c). The upstream temperature fluctuations have relatively more power in the low frequency range than that in the high frequency range. The opposite holds for downstream temperature fluctuations. The branch jet reaches the bottom wall more intermittently upstream. Hence, the deviation in the temperature spectra at x/δ=2.0 in Fig. 10 (b) implies that the mean attachment point of the branch jet on the bottom wall lies a slightly farther downstream in the simulation. This can be attributed to both the higher Prandtl number and the effects of the buoyancy.

CONCLUSIONS

In the present study, direct numerical simulation and experiments of turbulent thermal mixing around the T-junction are carried out. Following conclusions are drawn.

1. The mean and RMS velocities in the main-flow and vertical directions from the simulation with the fine grid system agree quantitatively well with the experiments everywhere in the neutral case. The mean and RMS temperature in the simulation are also in quantitative agreement with that in the experiments upstream (x/δ=1.0), although the deviation increases farther downstream owing to the difference in the Prandtl numbers. In contrast, only qualitative agreement is achieved in the simulation with the coarse grid systems.
2. The buoyancy alters the mean velocity and temperature distribution dramatically in the strongly stable/unstable case (Ri=±9.3). On the other hand, the effects of buoyancy are limited to where the magnitude of the vertical velocity is low at Ri=±0.93.
3. The RMS temperature on the bottom wall for the smaller absolute Richardson number is higher in the downstream region. The peak-to-peak amplitude of temperature there is six times higher than the RMS temperature. The value approaches 1 at the maximum RMS temperature position near the leading edge of the branch duct.
4. Flow visualization reveals that the skewed temperature fluctuations on the duct walls are caused by various kinds of large-scale coherent structures, such as a groove on the branch jet, upper and lower kidney vortices, separation in the branch duct and roll-ups shed from the leading and trailing edges of the duct, near the junction.

REFERENCES

[1] Kawamura, T., Shiina, K., Ohtuska, M., Tanaka I., Hirayama, H., Tanimoto, K., Fukuda, T., Sakashita, A. Mizutani, J., Minami, Y., Moriya, S. and Madarame, H., "Experimental Study on Thermal Striping in Mixing Tees with Hot and Cold Water," Proc. 10th Int. Conf. Nuclear Engineering, Arlington, VA, in CD-ROM (2002), ICONE10-22214, pp. 1-8.

[2] Sierra-Espinosa, F. Z., Bates, C. J. and O'Doherty, T., "Turbulent Flow in a 90° Pipe Junction Part1: Decay of Fluctuations Upstream the Flow Bifurcation," Computers & Fluids, Vol. 29, No. 2 (2000), pp. 197-213.

[3] Simoneau, J.-P., Noe, H. and Menant, B., "Large Eddy Simulation of Sodium Flow in a Tee Junction - Comparison of Temperature Fluctuations with Experiments, " Proc. 8th Int. Topical Meeting on Nuclear Reactor Thermal-Hydraulics, Kyoto, Japan, Vol. 3 (1997), pp. 1404-1411.

[4] Fukushima, N. and Kasagi, N., "DNS of Fully Developed Turbulent Fluid Flow and Heat Transfer in a Duct of a Quadrilateral Cross Section," Proc. 14th Symposium on Computational Fluid Dynamics, Tokyo, Japan, (in Japanese), in CD-ROM (2000), pp. 1-5.

[5] Rai, M. M. and Moin, P., "Direct Simulations of Turbulent Flow Using Finite-Difference Schemes," J. Comp. Phys., Vol. 96 (1991), pp. 15-53.

[6] Le, H. and Moin, P., "Direct Numerical Simulation of Turbulent Flow over a Backward-Facing Step," Rep. TF-58, Ph. D. thesis, Stanford University, 1994.

[7] Kelso, R. M., Lim, T. T. and Perry, A. E., "An Experimental Study of Round Jets in Cross-Flow," J. Fluid Mech., Vol. 306 (1996), pp. 111-144.

[8] Takahashi, S., Shiina, K., Mizushina, Y., Asada, Y., Fujimura, H. and Nakamura, S., "Thermal Mixing Characteristics of Two Fluid Flows with Different Temperatures in a T-tube," Trans. JSME, (in Japanese), Vol. 63, No. 613, B (1997), pp. 2970-2976.

[9] Andreopoulos, J., "Measurements in Jet-pipe Flow Issuing Perpendicularly into a Cross Stream," Trans. ASME I: J. Fluids Eng. Vol. 104 (1982), pp. 493-499.

[10] Schlüter, J. U. and Schönfeld, T., "LES of Jets in Cross Flow and Its Application to a Gas Turbine Burner," Flow, Turbulence and Combustion, Vol. 65 (2000), pp. 173-203.

[11] Cortesi, A. B., Yadigaroglu, G. and Banerjee, S., "Numerical Investigation of the Formation of Three-Dimensional Structures in Stably-Stratified Mixing Layers," Phys. Fluids, Vol. 10, No. 6 (1998), pp. 1449-1473.

[12] Lim, T. T., New, T. H. and Luo, S. C., "On the Development of Large-Scale Structures of a Jet Normal to a Cross Flow," Phys. Fluids, Vol. 13, No. 3 (2001), pp. 770-775.

[13] Yuan, L. L., Street, R. L. and Ferziger, J. H., "Large-Eddy Simulations of a Round Jet in Crossflow," J. Fluid Mech., Vol. 379 (1999), pp. 71-104.

[14] Kelso, R. M. and Smits, A. J., "Horseshoe Vortex Systems Resulting from the Interaction between a Laminar Boundary Layer and a Transverse Jet," Phys. Fluids, Vol. 7, No. 1 (1995), pp. 153-158.

[15] Fric, T. F. and Roshko, A., "Vortical Structure in the Wake of a Transverse Jet," J. Fluid Mech., Vol. 279 (1994), pp. 1-47.

[16] Haven, B. A. and Kurosaka, M., "Kidney and Anti-Kidney Vortices in Crossflow Jets," J. Fluid Mech., Vol. 352 (1997), pp. 27-64.

Copyright © 2003 JSME